 CMES, vol.23, no.1, pp.53-73, 2008

Consolidation of a Soft Clay Composite: Experimental Results and Computational Estimates

A.P.S. Selvadurai[1] **and H. Ghiabi**[2]

Abstract: This paper deals with the problem of the consolidation of a composite consisting of alternate layers of soft clay and a granular material. A series of experiments were conducted on components to develop the constitutive models that can be implemented in a computational approach. The constitutive response of the soft clay is represented by a poro-elasto-plastic Cam clay-based model and the granular medium by an elasto-plastic model with a Drucker-Prager type failure criterion and a non-associated flow rule. The computational poro-elasto-plastic model is used to calibrate the experimental results derived from the one-dimensional tests and to establish the influence of the volume fractions and spatial arrangement of the soft clay and the granular material on the consolidation response. The computational developments are extended to examine certain idealized situations involving clay inclusions that are distributed within a granular medium in a regular arrangement.

Keyword: Soft clay, composite fill, poro-elasto-plastic geomaterials, clay lump, experimental study, computational modeling

1 Introduction

Although isotropy and homogeneity are dominant assumptions of geotechnical analysis there are situations where these assumptions are not true representations of geotechnical practice (Booker and Small, 1987; Seyrafian et al., 2006; Selvadurai, 2007a). The paper by Eden (1955) discusses the presence of varved features in clay specimens obtained from Steep Rock Lake, Ontario. Periodic deposition of eroded material in lacustrine environments can lead to geological deposits with anisotropy in strength and deformability characteristics. Examples of natural inhomogeneity in the deformability characteristics of London Clay was reported by Ward et al. (1965). Inhomogeneities can also be deliberately introduced to enhance either the load carrying capacity of soft clays or to improve their rate of consolidation. Stone columns or lime-stabilized columns are instances where the stiffer inclusion provides the reinforcement for strength and the reduction of settlements, while the incorporation of geosynthetics and sand layers are there to enhance the rate of consolidation of the construction. The theoretical, computational, laboratory experiments and field studies in this area are far too numerous to outline in detail. The reader is referred to the articles, volumes and reviews by Gibson (1967), Gibson et al. (1971), Hughes and Withers (1974), Madhav and Vitkar (1978), Mitchell and Huber (1985), Schweiger and Pande (1986), Canetta and Nova (1989), Tan et al. (1992), Lee and Pande (1998) and Selvadurai (2007a).

The major emphasis of this paper relates to a different class of soil composite, which is encountered in land reclamation practices and involves the use of dredged clay lumps that are interspersed within granular materials. A common construction technique for these lumpy clay fills involves placing dredged clay lumps directly on top of other layers, without filling the void space with another material. As a result, the built up reclamation fill experiences substantial compression purely due to the reduction of the void space, quite apart from the consolidation of the clay lumps

[1] Corresponding author. William Scott Professor and James McGill Professor. Department of Civil Engineering and Applied Mechanics, McGill University, 817 Sherbrooke Street West, Montreal, QC, Canada H3A 2K6 E-mail: patrick.selvadurai@mcgill.ca; Tel: +1 514 398 6672; fax: +1 514 398 7361

[2] Doctoral student

themselves, and this renders the technique ineffective and unreliable unless account is taken of the large compression that can be associated with the void closure. Examples of such large compression of fills constructed with clay lumps are reported by Leung et al. (2001) and Robinson et al. (2005). After clay lumps have been deposited in the reclamation fills, two different mechanisms will contribute to the settlement of the lumpy fills. The first mechanism corresponds to the expulsion of fluid from the voids between lumps, inter-lump voids, while further settlement takes place due to the decrease in the void ratio of the soil lump, referred to as intra-lump voids. Callari and Federico (2000) implemented the double porosity approach, first used in the petroleum industry to model the flow in a fractured porous medium, to deal with the consolidation of structured clay fills. In this approach, the highly fissured porous medium was modeled as a double porosity continuous medium, in which the first system of pores represents the net of fissures besides the pores within the intact lumps. To validate the double porosity model, the results of the proposed model was compared with that of finite element computations. Furthermore, they conducted a number of experiments on structured clay samples consisting of an assembly of small cubical clayey blocks, each covered by a thin layer of geotextile. The comparison indicated that the theoretical double porosity curves reasonably agree with experimental and computational results, especially for settlement evolution. Yang et al. (2002) also used the double porosity approach to present an analytical solution for an idealized problem where a linear elastic soil subjected to self-weight and surcharge pressure. Subsequently, Yang and Tan (2005) implemented this formulation in finite element analysis considering non-linear void ratio against permeability and effective stress relations to ensure a more realistic prediction. This implementation was then used to analyze results from the two one-dimensional consolidation tests on a lumpy clay layer. Nogami et al. (2004) also developed a numerical method for consolidation analysis of lumpy clay fills, adopting the double porosity model and the meshless method based on "radial point interpolation" approach. The results of the proposed computational approach indicated good agreement with the results of finite element analysis which has been previously formulated for consolidation of fissured clay. An attempt was then made to model the behavior of the lumpy samples tested in the national university of Singapore (Wong, 1997); it was indicated that the double porosity model can reasonably predict the consolidation behavior of lumpy fills provided that proper material properties are given.

For a typical clay lump construction using, say, 1.5 m diameter clay lumps in cubic packing, the void closure can result in a compression strain of approximately 57%, which would be regarded as unacceptable if the fill is directly used for support of foundations. As a practical method to resolve this problem, the constructed fills are usually subjected to a surcharge load that accelerates the closure of the inter-lump voids (Karthikeyan et al., 2004). In order to achieve an effective compression from such a preloading process, the surcharge should be placed over the fill after the dissipation of any negative pore pressure that might be generated in the lumps due to the removal of overburden pressure particularly during dredging operation (Robinson et al., 2004). The construction time, therefore, could become longer depending on different factors such as size of the dredged lumps and the hydraulic conductivity of the fine-grained soil. An alternative to the aggregation of clay lumps is to fill the void space with a granular material that possesses a higher stiffness and a greater permeability thereby enhancing the load carrying capacity and minimizing the settlements and rate of consolidation of the composite, due to the reduction in the length of the drainage paths.

Reclaimed land that is constructed using clay lumps in conjunction with an interspersed granular fill is a *soil composite* and the mechanics of such composites are influenced by the constitutive properties of the individual phases, the interfaces between the phases and the associated volume fractions. This paper investigates the consolidation behavior of a composite consisting of disks of clay interspersed with layers of Ballotini. The experimental investigations are performed on a bench-scale oedometer with overall dimensions

measuring approximately 15 cm in diameter and 17 cm in height, with stacks of saturated clay interspersed with Ballotini of varying thickness. The experimental results are evaluated using a poro-elasto-plastic model for the saturated clay and an elasto-plastic model for the granular layers. The constitutive models are incorporated in the ABAQUS code in order to validate the computational approach to be used in further computational studies.

2 Materials and constitutive models

2.1 The silty clay

The fine-grained component of the composite specimen was reconstituted from lumps of silty clay obtained from an excavation located on Sherbrooke Street East (Montréal). A complete description of the preparation of the silty clay used in the bench-scale experiments is given by Ghiabi and Selvadurai (2006a).

The constitutive response of soft silty clays can be modeled by appeal to a variety of constitutive models (Desai and Siriwardane, 1984; Darve, 1990; Cambou and di Prisco, 2000). In this paper a Cam-clay model is chosen and the strength and stiffness parameters of the silty clay were determined from the results of CU (Consolidated Undrained) triaxial and conventional consolidation tests (Ghiabi and Selvadurai, 2006a). From the results of the two oedometric consolidation tests conducted on the reconstituted Montréal silty clay, the slope of the hydrostatic compression and swelling lines of the e vs. ln p curves were established at λ=0.0564 and κ=0.0104, while the stress ratio parameter, M, estimated from results of CU Triaxial Tests, was 1.55. Furthermore, using the method presented by Casagrande, the hydraulic conductivity of the silty clay was estimated from the results of the oedometer test to be in the range 1.3×10^{-8} cm/sec to 7.2 $\times10^{-8}$ cm/sec.

2.2 The granular medium

Ballotini, an artificial particulate medium consisting of glass beads manufactured by Potters Industries Inc. (La Prairie, Quebec; www.pottersbeads.com) was used as the granular component of the composite specimens. The Ballotini used was type A3 with a specific gravity estimated at G_S=2.5. The grain size analysis conducted on the supplied material indicated that 83% of this granular material ranged from 600μm to 850 μm, while approximately 17% had a particle size between 300μm and 600μm.

The constitutive behavior of particulate materials such as ballotini can be represented by a variety of models ranging from non-linear elastic models to hypoplasticity (Hill and Selvadurai, 2005). The range of applicability of a particular model will ultimately depend on the mode of application of the constitutive model and the ease with which the parameters describing the model can be determined through conventional tests. In this study, the mechanical behavior of the ballotini is modeled by appeal to a non-linearly elastic-perfectly plastic constitutive model with a non-associated flow rule. The specific model used to describe failure is a Drucker-Prager failure criterion defined by

$$f(\sigma_{ij}) = \sqrt{J_2} + \alpha_1 I_1 - \beta \tag{1}$$

and the plastic potential is chosen as

$$g(\sigma_{ij}) = \sqrt{J_2} + \alpha_2 I_1 \tag{2}$$

where I_1, J_2 are, respectively, the first and second invariants of the stress deviator tensor referred to effective stresses. The parameters of the constitutive model were determined from the results of a series of consolidated drained (CD) triaxial, bench-scale oedometer and isotropic compression tests conducted on ballotini specimens. The results indicated that the elastic stiffness of ballotini is highly dependant on the physical states of the material; a relation is presented as a bi-linear expression that defines the modulus of elasticity as a function of the void ratio. To incorporate the non-linear elastic approach with a plasticity concept, a computational procedure was developed: The first modification involved the sub-incremental procedure in calculation of the elastic deformation when the stress state lies within the yield surface. Hence, the elastic stiffness tensor $[C^e]$ was updated in each sub-increment based on

the constitutive relations presented for the stiffness parameters. After the stress state reached the yield surface, further stress increments were calculated considering the elastic-plastic stiffness tensor $[C^{ep}]$. In each sub-increment, the state of stress, determined from the new stiffness tensor and strain increment, was scaled back to the yield surface. When the nonlinear elastic behavior is considered for the material, this tensor was recalculated in each sub-increment based on the state of stress and state of strain, which can change the constitutive characteristics of the material. The hydraulic conductivity is another important parameter required in pore pressure diffusion- stress analysis. This parameter is estimated at 1.6×10^{-3} cm/s from the results of the constant head permeability tests conducted on the ballotini specimens. The parameters for the constitutive models used in the computational study are given in Table 1.

Table 1: Constitutive parameters used in computations

Ballotini (non-linear elastic perfectly plastic)		
Elastic modulus	$e > 0.605$	27000
E(kPa)	$e < 0.605$	$(6.24\text{-}10.25e) \times 10^6$
Poisson's ratio		0.3
α_1 (Eq. 1)		0.298
β (Eq. 1)		0
α_2(Eq. 2)		0.165
Hydraulic conductivity k (cm/s)		1.6×10^{-3}

Clay (Cam-clay model)	
Hydrostatic compression index λ	0.0564
Swelling index κ	0.0104
Poisson's ratio	0.3
Stress ratio M	1.55
Hydraulic conductivity k (cm/s)	2×10^{-8}

3 Experimental investigations

The experimental program described in this paper studies the behavior of a composite specimen, consisting of a coarse-grained medium interspersed with disk-shape clay inclusions subjected to bench-scale oedometer tests. The samples were fabricated in a consolidation cell with different numbers of silty clay disks placed within a granular region. The results of the oedometric compression test are used to assess the influence of the volume proportion of the fine-grained region, in relation to the granular medium, on the mechanical response of the entire sample. The experiments also provide useful data for comparison with the numerical results to determine the predictive capabilities of a computational approach.

3.1 Bench-scale experiments

The bench-scale experiments were designed for testing the composite soil specimens in which a controlled axial stress from static weights initiates the oedometric consolidation of the composites (Figure 1). A weight rack was designed to accommodate weight of up to 2.67 kN that could be added in loading increments. The initial stress on the sample was approximately 81 kPa and this was increased in subsequent loading sequences to 149, 219, 273, 383 and 493 kPa by adding weights in five loading steps. To minimize the development of dynamic effects in the loading process, the load was applied gradually using a scissor jack installed in the loading frame. Each load step lasted for approximately 24 hours, after which no excess pore pressure was expected to remain in the system; this limit was arrived at through a computational modeling of the experimental configuration.

The instrumentation used in the experimental setup included a load cell located on the top of the plunger and two LVDTs connected to the rectangular plate to measure the uniaxial compression of the sample (Figure 1). The load cell used in this experiment had a capacity of 10 kips (44.48 kN) with an accuracy equal to $\pm0.04\%$ FS. Two LVDTs, with a displacement range of 2.5 cm, were attached to opposite sides of the plunger to record the vertical compression of the specimen.

3.2 Sample preparation

Considering the consistency of the reconstituted clay paste, a PVC mold (internal diameter 12.5 cm, height 1.94 cm) with a PVC base plate

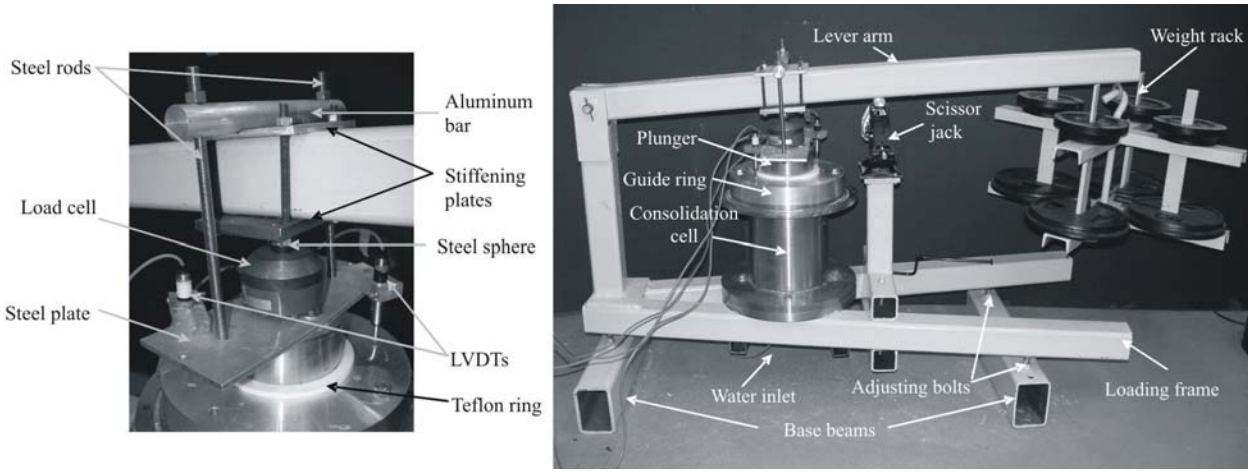

Figure 1: Loading setup and instrumentations used in the bench-scale test

(a) (b) (c) (d)

Figure 2: Preparation of the silty clay disks (a) PVC mold (b) Compacting clay paste with plunger (c) Trimming the clay disk using wire saw (d) Placing the molded clay in a sealed bag

was used to fabricate the clay discs (Figure 2a). To avoid air entrapment within the specimen, a plunger was used to slightly compact the soil paste inside the mold (Figure 2b) and the top of the sample was trimmed using a wire cutter (Figure 2c). The mold containing the specimens were then placed in a sealed bag (Figure 2d) and stored at a temperature of -10°C for 24 hours, after which the frozen clay discs were removed from the mold. The shape of the discs and their water content was maintained by re-freezing them in sealed bags. The moisture content determined from tests on frozen clay disks indicated that the specimens were at, approximately, the liquid limit of the silty clay (25%). This value is lower than the range of 30% to 50% which is reported as moisture content of the dredged lumps in different reclamation projects. Due to the high silt content, the reconstituted silty clay has a low liquid limit and plasticity index; therefore, the soil with 30% to 50% moisture content will be in form of slurry. Since the clay lumps dredged from the seabed tend to have the consistency of a slurry, the soil paste with approximately 25% moisture content was used in the experimental study, which showed good consistency during sample preparation.

The composite soil specimens were prepared in the cylindrical cell of the bench-scale setup with an internal diameter of 15.2 cm. The samples (approximate height 16.8 cm) contained either four, six or eight disks of clay with the volume fraction evaluated at 31%, 47% and 62.5%, respectively. The disks were spaced at equal distances and the ballotini was dispersed and slightly compacted in layers to construct the soil composite (Figure 3); the amount of ballotini used in the composites was measured for estimating the initial physical state of the granular part of the composite. The composite samples were saturated with deaired wa-

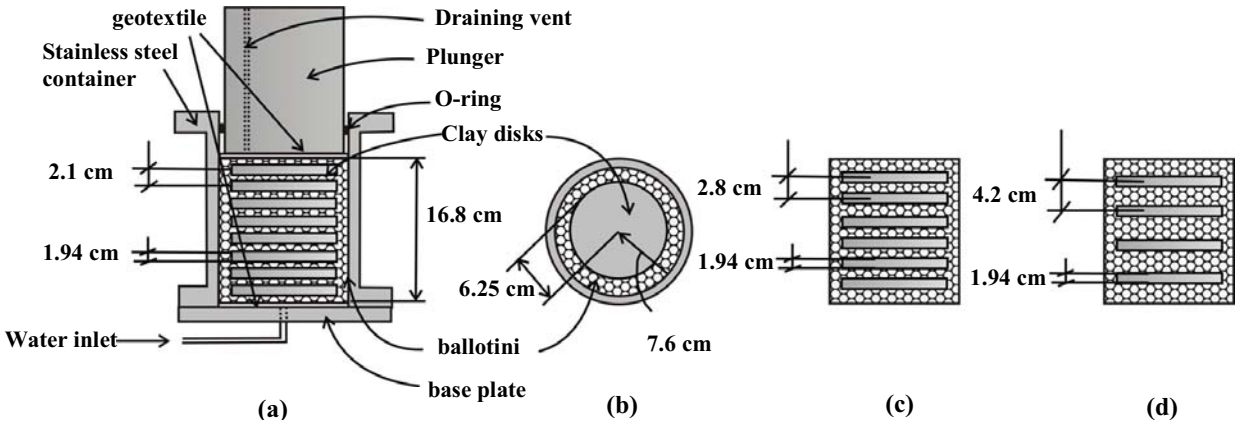

Figure 3: (a) Cross sectional view of the 8-disk composite sample (b) Planar cross section (c) the 6-disk composite sample (d) the 4-disk composite sample

ter prior to application of the load, and the water level was maintained at the upper level of the samples for a period of two days. During application of the axial load, proper drainage was assured by placing two layers of geotextile at the upper and lower surfaces of the samples, which were connected to the draining vent and water container, respectively.

3.3 Experimental results

The measurement of the axial compression of the composite specimens forms an important component of the experimental results that will be used in the calibration of the computational predictions. A further bench-scale test was conducted on a pure ballotini sample to assess the influence of the volume proportion of clay inclusions on the mechanical properties of the composites. Figure 4 shows a comparison of the time-dependent settlement response of the three samples of the composites compared with that of a pure ballotini specimen. The tests indicate that an increase in the volume proportion of clay results in a higher axial compression of the composites; the axial settlement of the four-disk sample at the end of the final load step was 2.8 times that of a pure ballotini specimen. Furthermore, at the termination of the last load step, the eight-disk sample exhibits approximately five times more axial compression than that experienced by a pure ballotini sample. The experimental results also show a progressive axial compression at the end of each load step: This phenomenon is mainly related to the time-dependent compression of ballotini due to the internal re-arrangement of the granular assembly. Such time-dependent behavior in granular media, particularly when they are used in low density conditions in laboratory investigations, has been observed, among others, by Murayama et al., (1984), Lade (1994), Di Prisco and Imposimato (1996) and Kuwano and Jardine (2002) and further discussed in the article by Ghiabi and Selvadurai (2006b). Comparing the results of different tests, it was shown that this phenomenon was diminished in the tests conducted on fabricated samples with a lower volume of ballotini; therefore, in the six- and eight-disk composites, an ultimate compression state was observed at the end of the load steps.

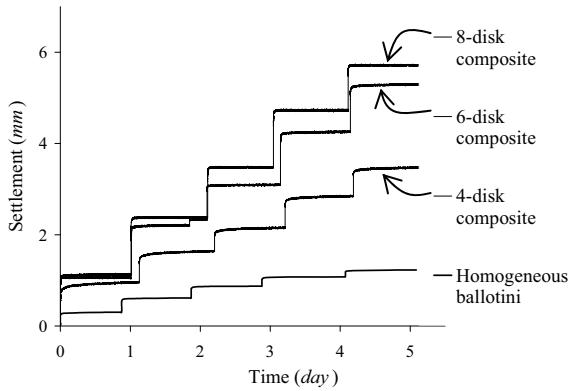

Figure 4: Axial settlement of the samples in five successive load steps

During the axial loading of the soil composites, a mixture interface can develop at the boundary of the two materials as a result of penetration of the ballotini particles into the soft clay. In this study, the development of this mixture interface was investigated by dissecting the composite samples at the termination of the tests. These investigations indicated that there was no measurable penetration of the ballotini grains into the soft clay disks at this stress level, although a layer of ballotini beads had adhered to the surface of the disks; these could be easily removed from the clay surface. The issue of particle penetration and its influence on the consolidation response of the clay in terms of alteration of the fluid transport boundary conditions at the interface was recently investigated by Selvadurai (2007b), using an idealized model of contact of discs at an interface. For both hexagonal and cubic arrangements of the contacting discs, the consolidation rate exhibits a marginal change but the total consolidation deformations are uninfluenced.

4 Computational modeling of fluid-saturated media

4.1 Constitutive equations

Many geotechnical engineering problems include time-dependent mechanical responses of soil media associated with the expulsion of the pore fluid pressure, which depends on hydraulic properties of the material and the associated boundary conditions. To account for this behavior it is necessary to couple the equations governing mass conservation, the flow of pore fluid through the soil skeleton, the constitutive equations governing the mechanical behavior of the soil skeleton and the equations of equilibrium.

In this section we examine the poro-elasto-plastic modeling of the time-dependent response of the clay composite. The poro-elasto-plastic modeling extends the classical theory of poroelasticity developed by Biot (1941) to include effects of failure of the porous soil skeleton and the attendant alterations in the stiffness and fluid transport properties of the soil skeleton. The extensions of poroelasticity to include failure, yield, damage and viscoplasticity of the soil skeleton has found many useful applications, particularly in the area of geomechanics, biomechanics, energy resources exploration and environmental geotechnique. The literature in these areas is extensive and no attempt is made to provide a comprehensive survey of the topics. The review articles and volumes by Cheng and Dusseault (1993), Coussy (1995), Selvadurai (1996, 2007b), Lewis and Schrefler (1998), Thimus et al. (1998), Auriault et al. (2002), Ehlers and Bluhm (2004) and Selvadurai and Shirazi (2005) can be consulted for up-to-date literature.

Under the assumption of small-strain theory, the equation of equilibrium for quasi-static conditions can be written as

$$\nabla.\boldsymbol{\sigma} + \rho\mathbf{g} = 0 \tag{3}$$

where $\boldsymbol{\sigma}$ is the total stress tensor and ρ is the average density of the multiphase system defined as

$$\rho = (1-n)\,\rho^s + n\rho^w \tag{4}$$

where ρ^s and ρ^w are, respectively, densities of the solid phase and water, n is the porosity and $\mathbf{g}$ is an acceleration vector usually related to the gravitational effects. Considering the Darcy's law for the flow through the porous skeleton and the incompressibility of the pore fluid, the mass conservation equation for the pore fluid in a saturated medium can be stated in the form

$$\nabla.\mathbf{v^s} + \nabla.\left[\frac{\mathbf{k}}{\mu^w}\left(-\nabla P^w + \rho^w\mathbf{g}\right)\right] = 0 \tag{5}$$

where $\mathbf{v^s}$ is the velocity vector of soil skeleton, $\mathbf{k}$ is the permeability tensor and P^w and μ^w are the isotropic pressure and viscosity of the fluid phase, respectively. The constitutive relationship of the skeleton is the additional equation that has to be considered in the analysis of the porous medium. Using the principle of effective stress, the constitutive equation can be written in the incremental form:

$$\Delta\boldsymbol{\sigma} = \mathbf{D}'\,\Delta\boldsymbol{\varepsilon} + \Delta\boldsymbol{\sigma}_\mathbf{f} \tag{6}$$

where $\mathbf{D}'$ is the effective elasto-plastic constitutive tensor, $\Delta\boldsymbol{\sigma}$ and $\Delta\boldsymbol{\varepsilon}$ are incremental total stress and incremental strain tensors, $\Delta\boldsymbol{\sigma}_f^{\mathbf{T}} = \{\Delta P^w, \Delta P^w, \Delta P^w, 0, 0, 0\}$ in which ΔP^w is the change in pore fluid pressure.

4.2 Finite element formulation for consolidation problem

Complete expositions of the general approach for computational modeling of poro-elasto-plastic media are given by Lewis and Schrefler (1998), Potts and Zradković (2001) and in the manuals associated with the general purpose finite element code ABAQUS (ABAQUS/Standard, 2006). The salient equations are briefly summarized for completeness.

The equilibrium condition can be expressed by considering the principle of minimum potential energy. The essence of the finite element method is to discretize the domain of interest into elements; therefore, minimizing the sum of the potential energy of the elements with respect to incremental nodal displacements gives a set of equations of the form:

$$\mathbf{K^G}\Delta\mathbf{d_n^G}+\mathbf{L^G}\Delta\mathbf{P_n^{wG}}=\Delta\mathbf{R^G} \tag{7}$$

where $\mathbf{K^G}$ is the global stiffness matrix, $\mathbf{L^G}$ is the off diagonal sub-matrix in the consolidation stiffness matrix, $\Delta\mathbf{R^G}$ is the incremental vector of global nodal forces, and $\Delta\mathbf{d_n^G}$ and $\Delta\mathbf{P_n^{wG}}$ contain the list of nodal displacements and fluid pressure of all nodes of the domain, respectively. Using the principle of virtual work, the governing equation can be written in finite element form as:

$$\mathbf{L^{GT}}\left(\frac{\Delta\mathbf{d_n^G}}{\Delta t}\right)-\Phi^{\mathbf{G}}\mathbf{P_n^{wG}}=\mathbf{n^G}+\mathbf{Q} \tag{8}$$

where $\mathbf{Q}$ represents any sources or sinks, and $\Phi^{\mathbf{G}}$ is the permeability sub-matrix in the consolidation stiffness matrix defined as:

$$\Phi^{\mathbf{G}}=\sum_{i=1}^{N}(\Phi^{\mathbf{E}})_i=\sum_{i=1}^{N}\left(\int_V\frac{\mathbf{E^T kE}}{\gamma_f}dV\right)_i \tag{9}$$

and

$$\mathbf{n^G}=\sum_{i=1}^{N}\left(\mathbf{n^E}\right)_{\mathbf{i}}=\sum_{i=1}^{N}\left(\int_V\mathbf{E^T ki^G}dV\right)_i \tag{10}$$

where the matrix $\mathbf{E}$ contains derivatives of the pore fluid interpolation function, γ_f is the unit weight of the fluid, $\mathbf{i^G}$ is the unit vector with opposite direction to gravity and ^{T} denotes the transpose. In this study, the general purpose finite element program ABAQUS/Standard was used to perform numerical simulations of the mechanical behavior of composite models composed of two different materials. This program has the capability to characterize constitutive properties of materials using a user-defined material subroutine (UMAT). ABAQUS implements the direct approach in coupling the effect of transient flow of the pore-fluid and the stress-strain behavior of the soil skeleton; thus, Equations (7) and (8) can be written in the following incremental form:

$$\begin{bmatrix}\mathbf{K^G} & \mathbf{L^G}\\ \mathbf{L^{GT}} & -\beta\Delta t\Phi^{\mathbf{G}}\end{bmatrix}\begin{bmatrix}\Delta\mathbf{d_n^G}\\ \Delta\mathbf{P_n^{wG}}\end{bmatrix}=\begin{Bmatrix}\Delta\mathbf{R^G}\\ \left(\mathbf{n^G}+\mathbf{Q}+\Phi^{\mathbf{G}}\left(\mathbf{P_n^{wG}}\right)\right)\Delta t\end{Bmatrix} \tag{11}$$

where β is the parameter used for the approximation in the flow equation. In order to ensure stability of the time marching process, it is necessary to choose $\beta\geq 0.5$(see e.g. Selvadurai and Nguyen, 1995; Lewis and Schrefler, 1998). ABAQUS considers a fully implicit scheme ($\beta=1$) to ensure the numerical stability of the analyses. These equations form the basis of the iterative solution of a time step in a coupled flow deformation analysis in ABAQUS/Standard.

4.3 Computational analysis of soil composites

The computational modeling of the oedometric compression of the composite samples was conducted using the general-purpose finite element code, ABAQUS/ Standard. Composite models that include both ballotini and clay disks are axisymmetric models whereas the UMAT subroutine used for ballotini was based on a three-dimensional formulation. In order to reduce the computational time for modeling the composite region, only a sector region with an angle of 22.5°was modeled. This region could be easily discretized into brick elements. The finite element mesh discretizations of the composite domains used in this analysis are shown in Figure 5. In this study a 20-node brick element (C3D20RP)

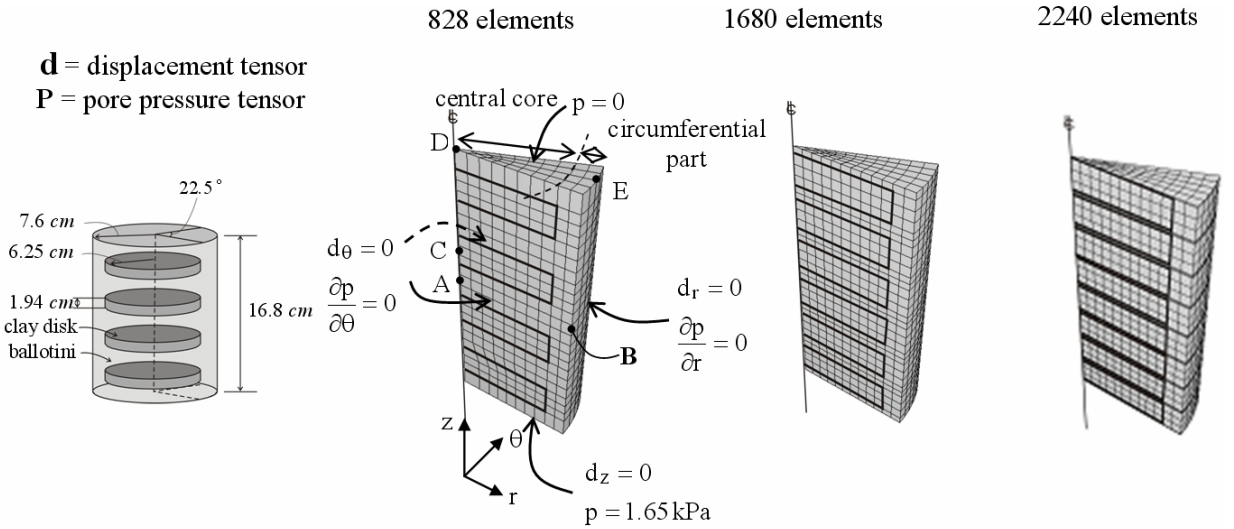

Figure 5: (a) Schematic figure of 4-disk sample (b) mesh configuration and boundary conditions- 4-disk sample (c) mesh configuration- 6-disk sample (d) mesh configuration- 8-disk sample

with quadratic variations in the displacement and linear variations in the pore pressure was selected, which employed a reduced integration scheme. The boundary conditions in the modeling, which were defined to represent the oedometric condition, are shown in Figure 5. The lateral boundaries were constrained horizontally with no provision for drainage; since drainage was provided through the geotextile layers and drainage vents, the upper and lower surfaces of the specimens were assumed to be free draining. Furthermore, the pore pressure at the upper and lower surfaces was assigned as zero and 1.65 kPa, respectively, since during the experiments the water level in the container was maintained at the same level as the top surface of the specimens.

Another phenomenon that takes place in lumpy fills is swelling of the clay lumps due to the suction that occurs when the clay lumps are subjected to a stress level after being consolidated under higher stress state (Robinson et al., 2004). In composite fills, it is assumed that the granular filler material is placed immediately after placement of the clay lumps. In other words, the suction process progresses while the lumps are enclosed within the granular phase. As a result, the existence of the filler phase can constrain the free swelling of the lumps due to confining stresses induced by the interaction between the two regions. The magnitude of the contact stress and the extent of the swelling process are, therefore, related to the stiffness characteristic of both materials. In this research, the material representing the fine-grained component, is a normally consolidated silty clay reconstituted in the laboratory (Ghiabi and Selvadurai, 2006a). The clay lumps, prepared from reconstituted clay paste, contain no negative pore water pressure and, therefore, the swelling process was not considered to be important in the experimental investigations and computations conducted on composite specimens as well as on composite lumpy fills.

The composite models were subjected to a uniform pressure applied to the upper surface, which increased from 81 kPa (initial load step) to 149, 219, 273, 383 and 493 kPa in six loading steps. The contact stresses between the plunger and the upper surface of the soil composite was modeled using the “rigid body” constraint option in ABAQUS.

In coupled pore fluid flow and stress analysis, the dissipation of the fluid pressure, initially generated within the pores of a porous media, gives rise to a gradual transfer of stress to the solid skeleton; this time-dependent response is required for full dissipation of the excess pore pressures. Figure 6 shows the variation of the pore fluid pressure in the last loading step for three points selected

from different locations of the four-disk composite sample (Figure 5), and indicate that the pore fluid pressure rises during the application of the axial load (the first second of the load step). The fluid pressure at point C, located inside the clay disk, increases by a greater magnitude than that computed for points A and B.

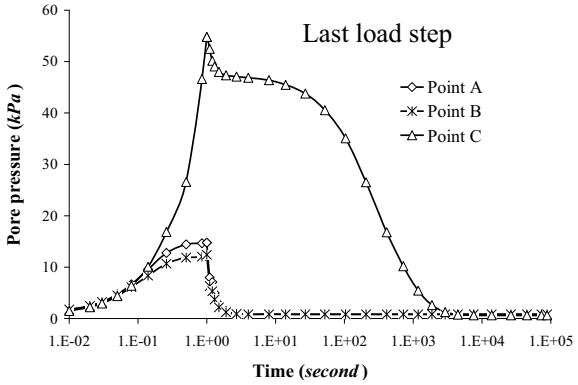

Figure 6: Pore fluid pressure change in different locations of four-disk composite model

After the axial pressure was applied in each load step, the axial load was maintained for 24 hours. The variation of pore fluid pressure at points A and B shows that no measurable excess pore pressure remained in the ballotini region 10 seconds after reaching the maximum axial load. Also, dissipation of the excess pore pressure in ballotini resulted in compression of the ballotini layers between the clay disks. The pore fluid pressure in the clay region was therefore primarily decreased due to a stress relaxation encountered in the central core of the composite, which can be verified by considering the variation of contact pressure computed at the top surface of the sample during any load step. Figure 7 shows the contact pressure change at points D and E (Figure 5) of the four-disk composite model during the last load step; here the vertical pressure applied to the central core gradually decreased, resulting in a rise of stress level within the outer annular part of the specimens. The computations also show that a considerable portion of the axial load was carried by the outer annular region surrounding the central composite core. In Figure 6 the excess pore fluid pressure generated within the clay parts was completely dissipated within 10000 seconds after the beginning of the load step, at which time the ultimate axial compression of the composite model was achieved.

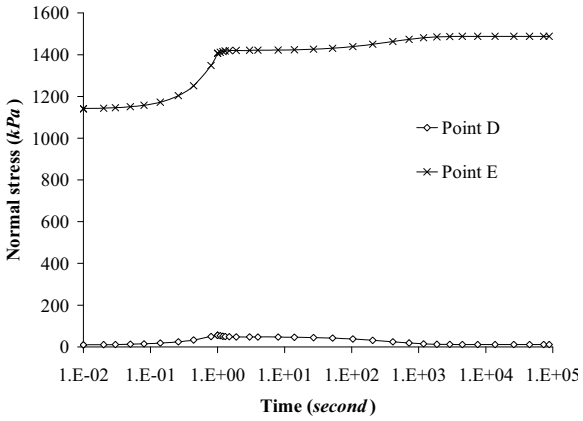

Figure 7: Variation of contact stress in four-disk model (last load step)

A progressive compression of the saturated porous samples occurred as a result of the time-dependent consolidation process in the constituents; the normalized axial compression in the last load step is presented in Figure 8. The computations show two different phases in the compression response of the composite; the first phase occurred due to dissipation of the fluid pressure trapped within the pores of the ballotini region, while the second phase was a result of the expulsion of the pore fluid from the pores of the clay inclusions. In addition, computational results indicate that in each load step 70% to 80% of the total settlement occurred during the first phase of the consolidation, which is referred to as the initial settlement.

4.4 Comparison between numerical predictions and experimental results

Computations were performed using the finite element models shown in Figure 5. The constitutive models developed for the constituents were implemented using the initial physical state of the materials, measured during the fabrication of the composite specimens. Figure 9 shows the comparison of the displacement-time responses between the computational predictions and the ex-

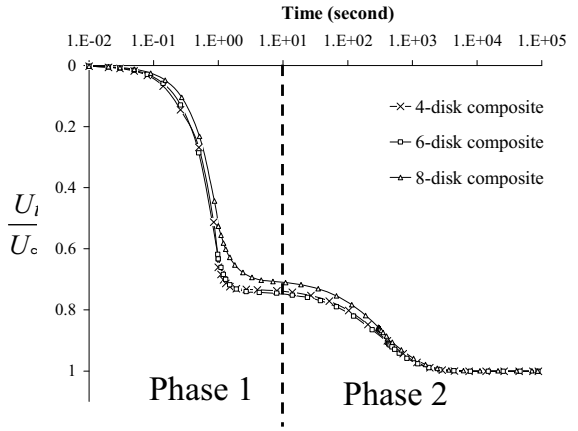

Figure 8: Axial compression of the composite models in the oedometric test (last load step)

perimental results. For the purposes of comparison, results are presented for three composite specimens (four-disk, six-disk, and eight-disk samples) subjected to an axial load that was increased in five consecutive load steps. It can be seen that the computational estimates predict, reasonably accurately, the experimental trends of load-displacement response for the three composite specimens tested. The axial settlement of the composite at the end of the last load step, predicted from computations is approximately 5% to 10% lower than the experimental responses. The

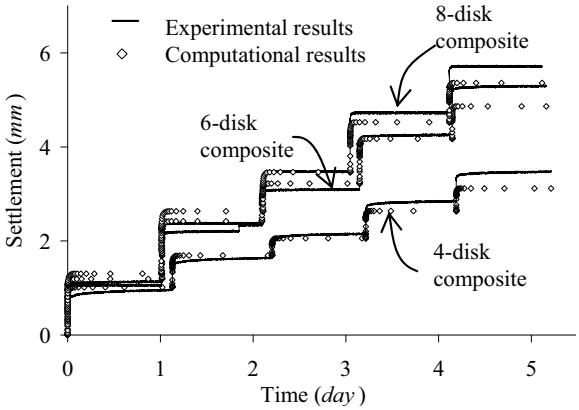

Figure 9: Axial compression of composite

hydraulic conductivity of the silty clay was estimated using the consolidation curves obtained from conventional oedometer tests. The experimental results indicated that this parameter is dependent on the void ratio of the material; the hydraulic conductivity evaluated from the first load step, in which the void ratio of the specimen reduced to about 0.57, was approximately 7.2×10^{-8}cm/s while it decreased to approximately 2×10^{-8}cm/s at the void ratio close to 0.46. Furthermore, in the central core of the composite specimens, that contained both soft silty clay disks and ballotini, a high proportion of the axial compression of the composite core occurs in the clay disks, and not in the ballotini phase placed between them, due to the relative stiffness properties of these constituents. Although higher compression was obtained by placing more clay disks within the composite, increasing the number of disks in the core region results in lower compression of each disk due to the increase in the volume of the soft soil. Therefore, lower compression of the clay inclusions gave rise to higher void ratio and hydraulic conductivity of the material.

Therefore, the computation attempts to predict the mechanical response of the composite samples considering two different values for hydraulic conductivity. The lower value was selected at 2×10^{-8} cm/s corresponding to void ratio of 0.46, and the higher limit was assigned a value 10 times higher than the lower one, which could be an estimation for the hydraulic conductivity when the soil has a void ratio higher than 0.57 (the initial void ratio of the normally consolidated silty clay is approximately 0.65). The results of the computational estimates and experimental investigations for the settlement-time curves are presented in Figure 10. Numerical estimations indicated that, after 10,000 sec, no excess pore pressure remained within the composites; therefore, it could be concluded that the ultimate consolidation settlement was achieved. In the four-disk sample reasonable correlation was obtained for the consolidation curves, although using the value of $k_{clay} = 2 \times 10^{-8}$ cm/s gave better predictions. In the six-disk and eight-disk samples, the experimental settlement curves shifted toward the numerical results obtained using the higher hydraulic conductivity for the silty clay material ($k_{clay} = 2 \times 10^{-7}$cm/s). Furthermore, in the eight-disk composite, there was a lower rate of consol-

idation during the first phase of the process. This phenomenon can be attributed to the slow dissipation of excess pore pressure generated in the ballotini layers located between the clay disks. Since the clay disks were placed approximately 1.6 mm apart, it is likely that contact between the disks results in the entrapment of fluid within the thin layers of ballotini. This results in a slower transfer of the load to the circumferential ballotini region and therefore a delay in the progress of the first phase of the consolidation process.

The experimental observations indicated that the time-dependent compression of ballotini results in further settlement of the sample after the termination of the consolidation process, a phenomenon that is more observable in the four-disk composite due to its higher volume proportion of ballotini. The reduction in the amount of ballotini in the six-disk and eight-disk specimens results in negligible time-dependent axial deformation after the termination of consolidation process.

5 The computational simulation of lumpy fill composites

In this computational study, different composite fills are simulated to investigate the influence of various parameters, on the consolidation response of lumpy fill composites. The dimensions of the composite domain and clay inclusions were selected by examining several typical projects reported in the literature (Hartlen and Ingers, 1981; Leung et al., 2001; Karthikeyan et al., 2004).

5.1 The composite lumpy fill

Using available information on the dimensions of the lumpy fills in different reclamation projects, cube-shaped lumps 1.5 m in width and 1.4 m in height (volume≈3.15 m^3) in a composite domain with a depth of 5.6 m was considered in the computational modeling; this domain can enclose three composite lumpy layers separated by the thin layers of ballotini. The composite medium is loaded by a 6 m square rigid footing placed on the surface of the fill. Due to symmetries associated with the problem only one-quarter of the domain is modeled, and to reduce the computational

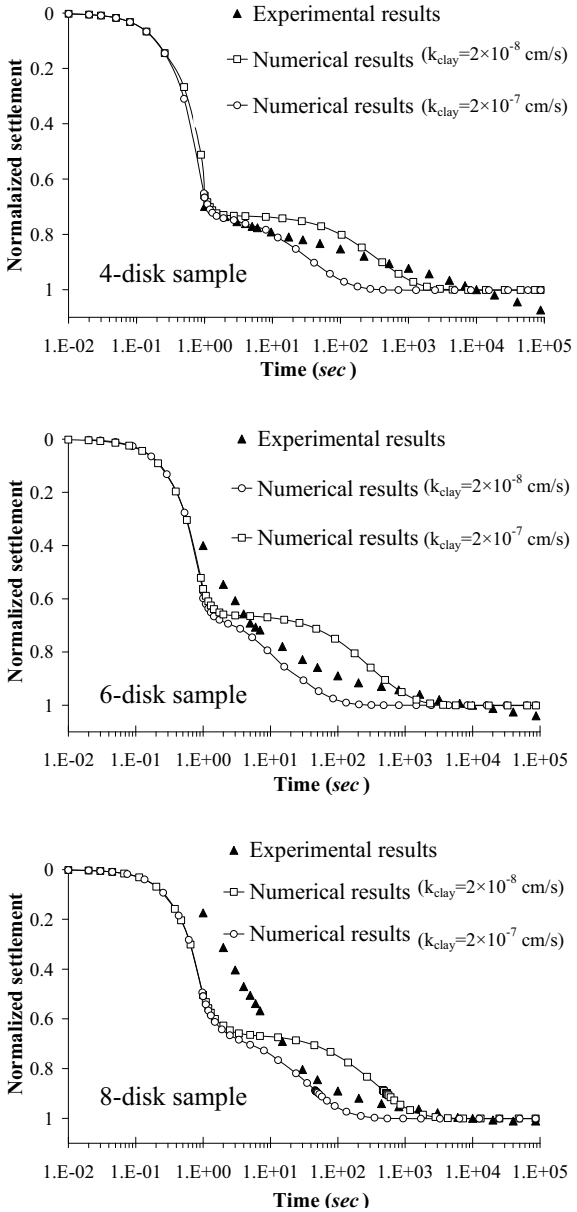

Figure 10: Consolidation curves of the three composite samples during the last load step σ_v = 493kPa

costs of performing the coupled pore fluid diffusion and stress analysis associated with an elastoplastic skeletal response, a domain with specific dimensions was selected where the boundary interface condition would not contribute appreciable influences on the results. In this numerical study, the size of the fill in both horizontal directions was set to 30 m with the vertical boundaries located 15 m away from the center of the footing.

Also in this study, the layers containing both ballotini and clay material were designated as *composite layers*. The composite fill can accommodate three composite layers; each can contain different volume portions of clay and ballotini. Figure 11 shows one of the composite layers that contains 25% volume proportion of the clay material, the remainder being the ballotini phase.

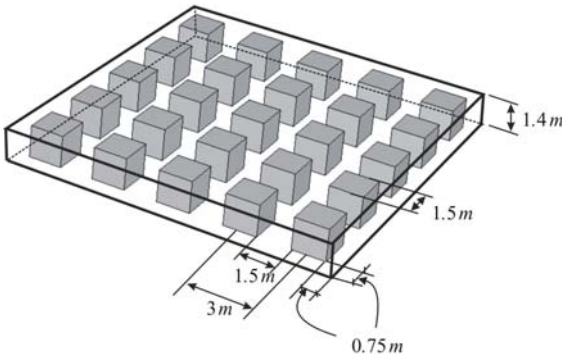

Figure 11: Composite layer with 25%volume fraction of clay

In land reclamation projects, a layer of surcharge is used to accelerate the consolidation process (Hartlen and Ingers 1981; Karthikeyan et al. 2004). The surcharge pressure and the self-weight of the deposited material are the loads that induce the initial state prior to the application of imposed structural loads, which in this case corresponds to a rigid footing. This computational study examines the mechanical responses of the composite models subjected to different loading steps. The first loading step includes the self-weight and a surcharge pressure of 90 kPa, (approximately corresponding to a layer of sand 5 m in height with a unit weight of 18 kN/m^3) gradually applied to the surface over a one day period. In the second loading step, a uniform pressure is applied to the square rigid footing; this uniform pressure is increased to 1500 kPa over a period of 25 min (rate of 1 kPa /sec) and then decreased to zero during the unloading step, which accounts for the irreversible deformation that occurs in the composite fill. In the reloading step the pressure is increased to 1500 kPa over a 25 min period, followed by the consolidation step, where the pressure on the footing is maintained at 1500 kPa, to allow for expulsion of excess pore pressures generated in the clay lumps and in the ballotini region. The duration of this consolidation step is set equal to 200 days after which there is virtually no excess pore pressure in the composite layer.

5.2 Composite fill with one composite layer placed at different locations

As the first part of the computational study, a single composite layer is placed at three different levels within the granular fill, denoted as **one-layer-B**, **one-layer-M**, and **one-layer-T**, as shown in Figure 12(a), (b) and (c). The boundary conditions chosen to model the displacement and pore pressure at the boundaries of the domain are shown in Figure 12 (d). The only permeable boundary with zero excess pore pressure defined in the model is the surface of the fill and all other boundaries are considered to be impermeable. The composite domains are discretized into 20-node brick elements with quadratic displacement and linear pore pressure formulations using a mesh discretization of 0.70 m in the vertical direction and 0.75 m in the horizontal direction, with all the clay lumps divided into 8 elements. The interface between the clay regions and the granular medium exhibits complete continuity in terms of the displacement and pore pressure fields. The computations can be used to predict the settlement of lumpy fills due to self weight and the pressure from the surcharge is used to induce pre-consolidation. These results indicate that soft lumps within the granular fill contribute to higher surface settlements, with the maximum occurring in the area over the clay lumps (Figure 13): In **one-layer-B** and **one-layer-M** fills, the profiles of the surface are almost identical, whereas the maximum settlement in **one-layer-T** fill shows an increase of approximately 28% due to the presence of soft clay lumps close to the surface.

The computations were extended to simulate the settlement of a 6m×6m rigid footing resting on the composite domain. The presence of a composite layer in the fill results in 20% to 25% greater initial settlement compared to that of a homogeneous ballotini fill (Figure 14). The results indicate that during a loading-unloading-reloading

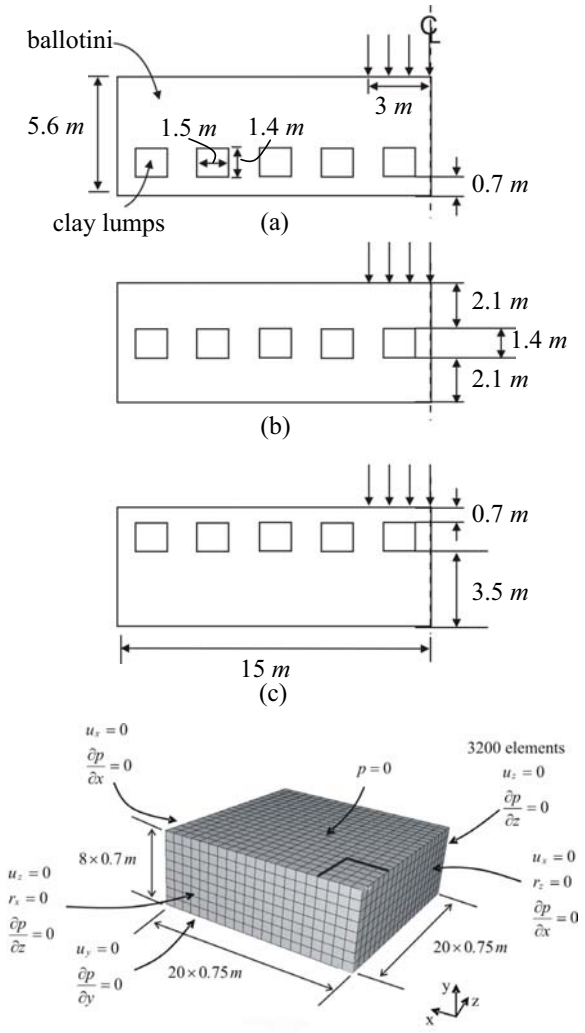

Figure 12: The location of composite layer in (a) 1-layer-B (b) 1-layer-M (c) 1-layer-T composite fills (d) mesh configuration and boundary conditions

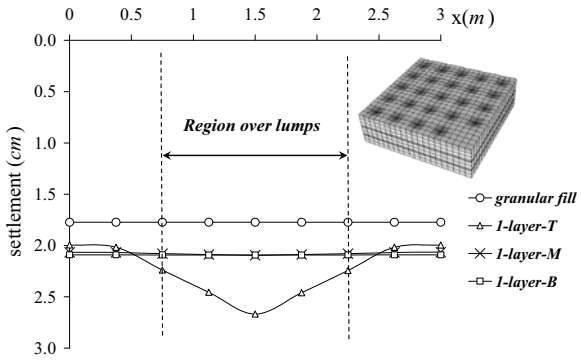

Figure 13: Surface settlement due to the application of gravitational load and surcharge pressure

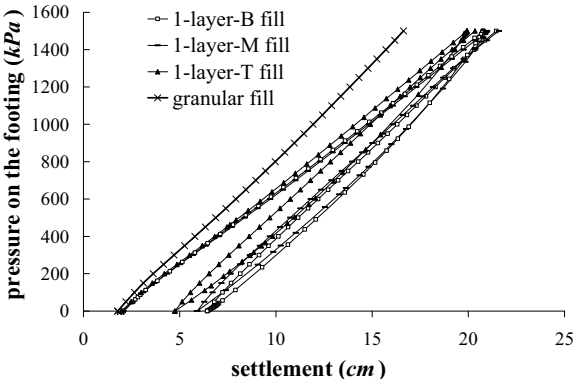

Figure 14: Load-settlement response of the rigid square footing resting on 1-layer composite fills

cycle, the initial settlement of **one-layer-B** and **one-layer-M** fills were about 21.5 cm while approximately 5% less settlement was obtained for the **one-layer-T** composite model.

Self weight effects, surcharge pressure and footing loads results in the generation of excess pore fluid pressure, particularly within the clay regions, and the dissipation of this excess pore fluid pressure induces further settlement of the footing during the consolidation step (200 days), and designated as the "consolidation settlement". Figure 15 compares the consolidation settlement for the different one-layer models: The first phase is complete within the first day and corresponds to the dissipation of the fluid pressure in the pores of the ballotini skeleton. This is followed by further settlement resulting from consolidation in the clay inclusions. The largest settlement in this step is 3.3 mm, occurring in the **one-layer-M** fill while the lowest occurs when the composite layer is located at the base of the fill (**one-layer-B**). These results indicate that the maximum total settlement is encountered when the composite layer is located at the half-depth of the fill.

5.3 Composite fills with different volume proportions of clay

To examine the effect of volume proportion of clay on the mechanical response of the composite fill, **two-** and **three-layer** composite fills are mod-

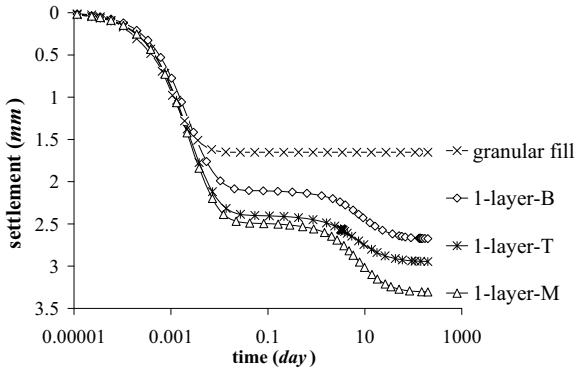

Figure 15: Consolidation settlement of a square rigid footing resting on 1-layer lumpy fills

eled (Figure 16). In the **two-layer** composite fill, the distance between two composite layers is 1.4 m, which is reduced to 35 cm in the **three-layer** fill. The mesh discretization and boundary conditions of **two-layer** composite models are identical to the **one-layer** model (Figure 12d). The mesh discretization used for the **three-layer** model is also shown in Figure 16d. The computations simulate the settlement of a rigid square footing on lumpy fills. The settlement of the rigid footing increases with the increase in the number of composite layers (Figure 17). As a result, the footing placed on the **three-layer** lumpy fill displays the highest initial settlement, approximately twice that for a homogeneous fill. Figure 17 also shows irreversible deformation after a complete loading–unloading cycle due to plastic deformation in both the clay lumps and granular filler: An increase in the number of lumps gives a higher irreversible settlement of the footing. At complete unloading, the **three-layer** lumpy fill had an irreversible displacement of 12.2 cm whereas the irreversible displacement in the **one-layer-B** fill was 6.4 cm. The computational results indicate that increasing the volume of the clay lumps gives a higher vertical displacement of the rigid footing during the consolidation step; the ultimate settlement of the rigid footing (in this study after 200 days) in a **three-layer** fill is approximately twice that of the **one-layer-B** fill. To investigate the influence of the volume proportion of clay on the mechanical response of the fills, the settlement of the footing is presented in terms of degree of consolidation U defined as:

$$U = \frac{\Delta(t) - \Delta(0)}{\Delta(\infty) - \Delta(0)} \tag{12}$$

where $\Delta(0)$ is the vertical settlement of the footing at the beginning of the consolidation step and $\Delta(\infty)$is the ultimate settlement (after 200 days). Figure 18 presents two different phases in the settlement response of the composite fills: The first phase corresponds to the quick consolidation of the ballotini region and the second phase is attributed to the consolidation process in the clay inclusions. By increasing the number of the lumps in the composite fill, the portion of settlement that occurs due to the consolidation of the clay lumps increases; in **one-layer-B** fill this represents 21% of the settlement, which rises to 36% in the **three-layer** composite region. The results also indicate that the consolidation settlement is delayed when the volume proportion of the clay lumps is increased; as a result, the time required for 50% and 90% consolidation, t_{50} and t_{90} is approximately three times longer in the **three-layer** fill compared to that of the **one-layer-B** model.

5.4 Composite fills with densely packed clay lumps

The composite layer used in the previous section to model the composite lumpy fills contained 25% volume fraction of lumps arranged in a square grid pattern (Figure 11). In order to investigate the influence of volume fraction and arrangement of clay lumps on the mechanical characteristics of the composite fills, a dense composite layer, containing 50% by volume of lumps arranged in a dense packing was considered (Figure 19). Two composite models are assembled, each with three dense composite layers located at the same depths used previously for the **three-layer** fill (Figure 16); the configuration of the dense composite models are shown in Figure 20, with either a cubical (**three-layer-D1**) or a hexagonal (**three-layer-D2**) packing. Thus, in the **three-layer-D2** fill, the lumps in the middle composite layer are only surrounded by ballotini. A mesh discretization identical to that shown in Figure 16d for the **three-layer** model is used for the new dense composite

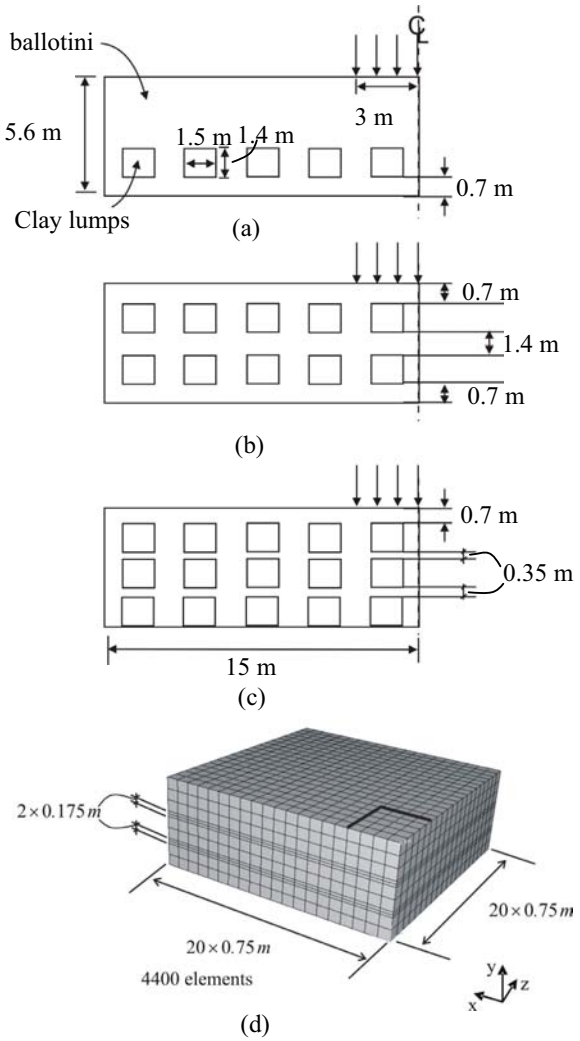

Figure 16: Locations of the composite layers in (a) 1-layer-B (b) 2-layer (c) 3-layer composites (d) mesh discretization of 3-layer model

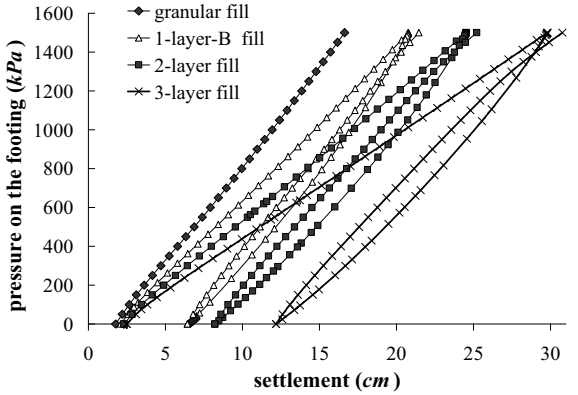

Figure 17: Load-settlement response of the rigid footing resting on different composite configurations

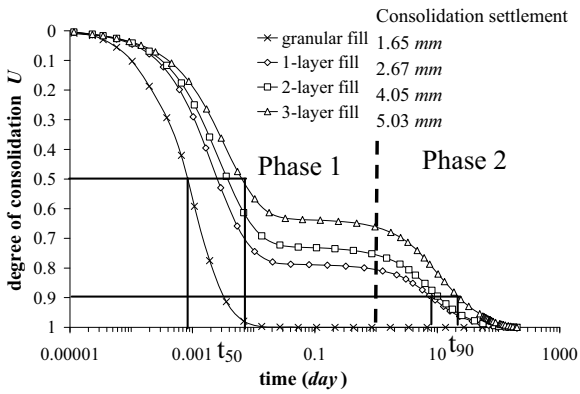

Figure 18: Normalized consolidation settlement of a footing resting on different lumpy fills

models. Other details of the simulations, such as boundary conditions and loading specifications, are identical to those implemented in the previous simulations. Figure 21 presents a comparison of the surface settlement profiles for **three-layer** composite fills (**three-layer**, **three-layer-D1** and **three-layer-D2**) due to self-weight and a uniform surcharge pressure, with the maximum initial surface settlement occurring in the area over the lumps of the top composite layer. The results indicate that increasing the volume proportion of soft clay in the fill results in a higher surface settlement. In **three-layer-D1** fill the maximum settlement is 5.1 cm, which is approximately 60% higher than that of **three-layer** composite fill. The maximum surface settlement computed in **three-layer-D2** fill is, however, 7.36 cm, indicating that larger surface settlement due to gravitational loads is obtained from a clay lump packing in a hexagonal form. Figure 22 shows the settlement responses of the footing placed on three different composite layers and subjected to uniform pressure up to a maximum of 1500 kPa. The initial settlement of the footing in dense packing composite layers is approximately 120% higher than that estimated for the **three-layer** composite fill, and can be attributed to the higher volume of clay present in the dense composite layer. During the loading step, the computations estimate the same magnitude of footing settlement for both

cubic and hexagonal and dense packing configurations; therefore, the difference of settlement predicted during the initial load step remains relatively unchanged until the termination of the loading step. After complete unloading, however, 40.8 cm of irreversible settlement is induced in the cubic packing **three-layer-D1** fill, which is 4.4 cm lower than that for the **three-layer-D2** fill.

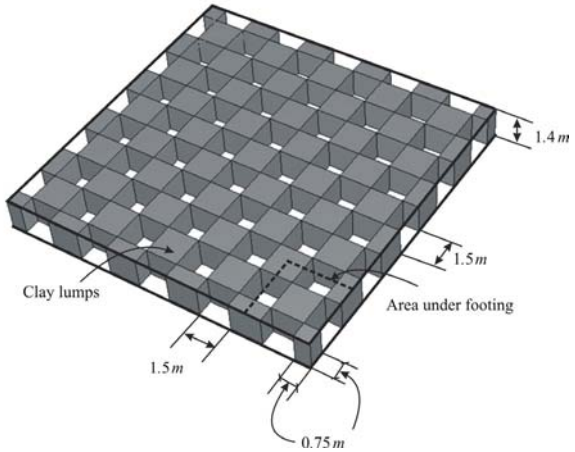

Figure 19: Locations of the clay lumps in dense composite layer

The settlement of the footing continues in the 200-day consolidation step due to the dissipation of the excess pore fluid pressure generated in the composite fills. The results indicate that the consolidation settlement of the footing in the **three-layer-D1** and **three-layer-D2** composite fills is 33.6 mm and 28.6 mm, respectively, which is approximately 6 times greater than that computationally estimated for the **three-layer** fill (Figure 23). It was also observed that in densely packed fills a higher portion of the consolidation settlement occurs in phase 2 due to consolidation of the fine-grained lumps. Figure 24 indicates that in densely packed lumpy fills, only 25% of the consolidation settlement takes place in phase 1 compared to 65% in loose packing layers. As a result the time period needed for 50% consolidation to occur in the densely packed fills increases to about 2.4 days compared to the 9 minutes estimated for **three-layer** fill.

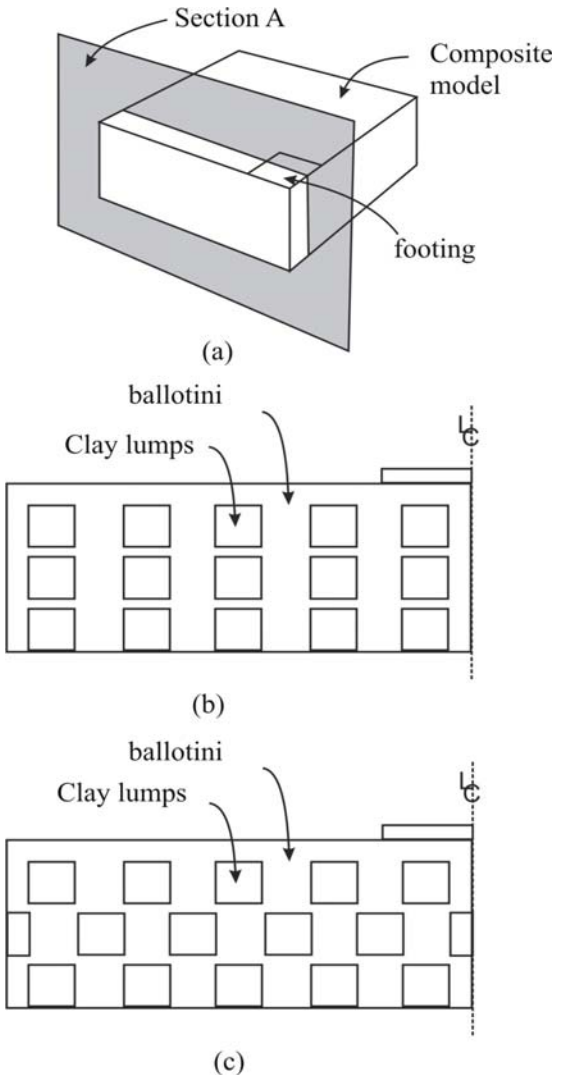

Figure 20: (a) location of section A in composite model (b) section A in cubical packing (3-layer-D1) (c) section A in hexagonal packing (3-layer-D2)

6 Concluding remarks

This study considered idealized lumpy soil regions where the voids between the lumps were filled with a type of granular material, which can enhance the mechanical characteristics of the lumpy material by eliminating the large void regions. The experimental program included bench-scale oedometer tests conducted on composite specimens with different volume proportions of clay and these showed that the presence of clay inclusions gives rise to higher axial compression

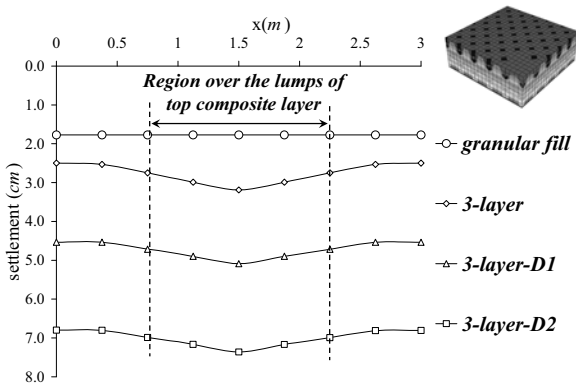

Figure 21: Profile of the surface settlement due to the application of self-weight and surcharge load

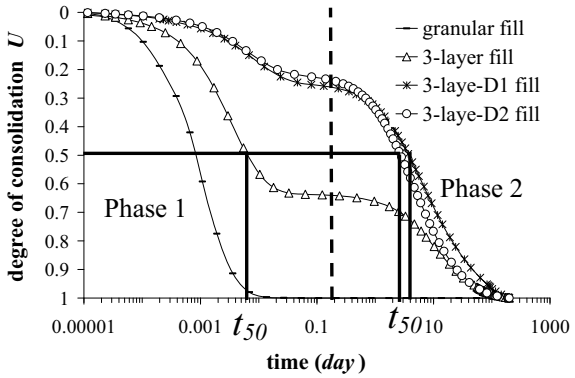

Figure 24: Degree of consolidation for 3-layer lumpy fills subjected to a footing load

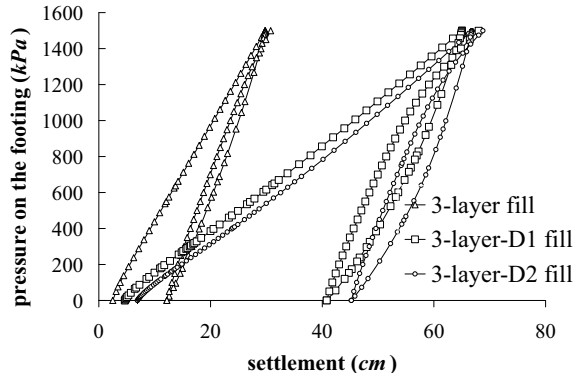

Figure 22: Load-settlement response of the rigid footing resting on 3-layer lumpy fills

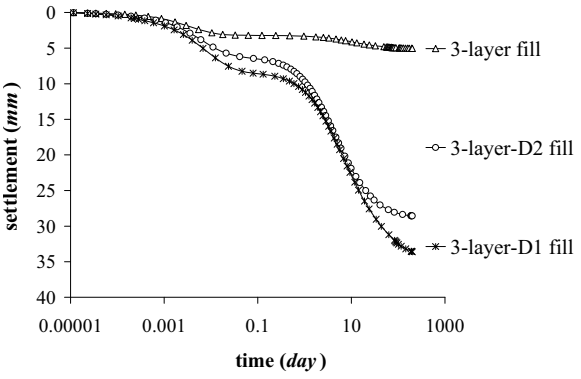

Figure 23: Consolidation settlement of a square rigid footing resting on composite lumpy fills

of the samples. A computational approach, validated with the experimental results, simulated the behavior of a large-scale composite fill of finite thickness subjected to self-weight, surcharge pressure, and loaded by a rigid footing. Computations showed that the response of a composite fill subjected to self-weight and surcharge pressure, is significantly influenced by the location of the lumps: The closer the lumps are to the surface the more uneven the surface settlement profile. The results indicted that the packing configuration of the lumps (hexagonal or cubical) can also induce different magnitudes of surface settlement.

The load-displacement response of a square rigid footing placed on composite finite-layer with various volume proportions of clay in relation to the granular phase was also examined. Increasing the volume proportion of clay inclusions gives rise to higher initial settlements and irreversible deformations take place during the loading and complete unloading cycles, respectively. After reloading and maintaining the pressure, the footing displays further settlements as a result of consolidation in the constituent soils within the composite fill. Increasing the volume proportion of fine-grained inclusions, both by placing more lumps in each composite layer, or by increasing the number of composite layers raises the settlement of the footing during the consolidation step. Furthermore, in composite layers with a higher volume of clay, the time-dependent settlement of the footing is delayed, which is attributable to the lower hydraulic conductivity of the clay material compared to that of the filler soil.

The experimental and computational results can be used to investigate the serviceability of com-

posite subsoils subjected to different types of loads. The most important case would be for reclaimed lumpy fills where the inter-lump voids are filled with a granular phase. The proposed computational scheme can be implemented to predict the mechanical behavior of the composite layers including the settlement and the time required to achieve ultimate deformation in the fills.

Acknowledgement: The work described in this paper was supported jointly by the *Max Planck Forschungspreis* awarded by the Max Planck Gesellschaft, Germany and the NSERC Discovery Grant awarded to the first author. The authors are grateful to a reviewer for the highly constructive comments and for drawing attention to further papers on the subject.

References

ABAQUS/Standard. (2006): A General-Purpose Finite Element Program. *Karlsson & Sorensen, Inc.*

Auriault, J.-L.; Geindreau, C.; Royer, P.; Bloch, J.-F.; Boutin, C.; Lewandowska, J. (Eds.) (2002): *Poromechanics II. Proc. 2th Biot Conference on Poromechanics*, A.A. Balkema, The Netherlands.

Biot, M.A. (1941): General theory of three-dimensional consolidation. *Journal of Applied Physics*, vol. 12(2), pp. 155-165.

Booker, J.R.; Small, J.C. (1987): A Method of Computing the Consolidation Behavior of Layered Soils Using Direct Numerical Inversion of Laplace Transforms. *International Journal for Numerical and Analytical Methods in Geomechanics*, vol. 11, pp. 363-380.

Callari, C.; Federico, F. (2000): FEM Validation of Double Porosity Elastic Model for Consolidation of Structurally Complex Clayey Soils. *International Journal for Numerical and Analytical Methods in Geomechanics*, vol. 24, pp. 367-402.

Cambou, B.; di Prisco, C. (2000): *Constitutive Modeling of Geomaterials*, Hermes Science Publishing Ltd, Oxford.

Canetta, G.; Nova, R. (1989): Numerical method for the analysis of ground improved by columnar inclusions. *Computers and Geotechnics*, vol. 7(1-2), pp. 99-114.

Cheng, H.; Dusseault, M.B. (1993): Deformation and diffusion behavior in a solid experiencing damage: a continuous damage model and its numerical implementation. *International Journal of Rock Mechanics and Mining Sciences & Geomechanics Abstracts*, vol. 30(7), pp. 1323-1331.

Coussy, O. (1995): *Mechanics of Porous Media*, John Wiley, New York.

Darve, F. (1990): *Geomaterials: Constitutive Equations and Modelling*, Elsevier Applied Science, London, New York.

Desai, C.S.; Siriwardane, H.J. (1984): *Constitutive Laws for Engineering Materials: With Emphasis on Geologic Materials*, Prentice Hall Inc., Englewood Cliffs, New Jersey.

Di Prisco, C.; Imposimato, S. (1996): Time dependent mechanical behaviour of loose sands. *Mechanics of Cohesive-Frictional Materials*, vol. 1(1), pp. 45-73.

Eden, W.J. (1955): Laboratory study of varved clay from Steep Rock Lake, Ontario, *American Journal of Science,* vol. 253(11), pp. 659-674.

Ehlers, W.; Bluhm, J. (2004): *Porous Media: Theory, Experiments and Numerical Applications*, Springer, Berlin.

Ghiabi, H.; Selvadurai, A.P.S. (2006a): Laboratory testing of a soft clay. *Fourth International Conference on Soft Soil Engineering* (Eds.: Chan, D.H.; Law, K.T.), Vancouver, pp. 447-456.

Ghiabi, H.; Selvadurai, A.P.S. (2006b): The time-dependent mechanical behaviour of a granular medium used in laboratory investigations. *International Journal of Geomechanics*, (under review).

Gibson, R.E. (1967): Some results concerning displacements and stresses in non-homogeneous elastic half-space. *Geotechnique*, vol. 17(1), pp. 58-67.

Gibson, R.E.; Brown, P.T.; Andrews, K.R.F. (1971): Some results concerning displacements in a non-homogeneous elastic layer. *Zeitschrift fuer Angewandte Mathematik und Physik*, vol. 22(5), pp. 855-864.

Hartlen, J.; Ingers, C. (1981): Land reclamation using fine-grained dredged material. *Tenth Int. Conf. Soil Mech. Found. Eng.*, Stockholm, pp. 145-148.

Hill, J.M.; Selvadurai, A.P.S. (2005): Mathematics and mechanics of granular materials. *Journal of Engineering Mathematics*, vol. 52, pp. 1-9.

Hughes, J.M.O.; Withers, N.J. (1974): Reinforcing of soft cohesive soils with stone columns. *Ground Engineering*, vol. 1(3), pp. 42-49.

Karthikeyan, M.; Dasari, G.R.; Tan, T.-S. (2004): In situ characterization of land reclaimed using big clay lumps. *Canadian Geotechnical Journal*, vol. 41(2), pp. 242-256.

Kuwano, R.; Jardine, R.J. (2002): On measuring creep behaviour in granular materials through triaxial testing. *Canadian Geotechnical Journal*, vol. 39(5), pp. 1061-1074.

Lade, P.V. (1994): Creep effects on static and cyclic instability of granular soils. *Journal of Geotechnical Engineering*, vol. 120(2), pp. 404-419.

Lee, J.S.; Pande, G.N. (1998): Analysis of stone-column reinforced foundations. *International Journal for Numerical and Analytical Methods in Geomechanics*, vol. 22(12), pp. 1001-1020.

Leung, C.F.; Wong, J.C.; Manivanann, R.; Tan, S.A. (2001): Experimental evaluation of consolidation of stiff clay lumps in reclamation fill. *Geotechnical Testing Journal*, vol. 24(2), pp. 145-156.

Lewis, R.W.; Schrefler, B.A. (1998): *The Finite Element Method in the Static and Dynamic Deformation and Consolidation of Porous Media*, J.Wiley & Sons, New York.

Madhav, M.R.; Vitkar, P.P. (1978): Strip footing on weak clay stabilized with a granular trench or pile. *Canadian Geotechnical Journal*, vol. 15(4), pp. 605-609.

Mitchell, J.K.; Huber, T.R. (1985): Performance of a stone column foundation. *Journal of Geotechnical Engineering*, vol. 111(2), pp. 205-223.

Murayama, S.; Michihiro, K.; Sakagami, T. (1984): Creep characteristics of sands. *Soils and Foundations*, vol. 24(2), pp. 1-15.

Nogami, T.; Wang, W.; Wang, J.G. (2004): Numerical Method for Consolidation Analysis of Lumpy Clay Fillings with Meshless Method, *Soils and Foundations,* vol. 44(1), pp. 125-142.

Potts, D.M.; Zdravković, L. (2001): *Finite Element Analysis in Geotechnical Engineering: Application*, Thomas Telford, London.

Robinson, R.G.; Dasari, G.R.; Tan, T.S. (2005): Three-dimensional swelling of clay lumps. *Geotechnique*, vol. 54(1), pp. 29-39.

Robinson, R.G.; Tan, T.S.; Dasari, G.R.; Leung, C.F.; Vijayakumar, A. (2004): Experimental study of the behavior of a lumpy fill of soft clay. *International Journal of Geomechanics*, vol. 5(2), pp. 125-137.

Schweiger, H.F.; Pande, G.N. (1986): Numerical analysis of stone column supported foundation. *Computers and Geotechnics*, vol. 2, pp. 347–372.

Selvadurai, A.P.S. (Ed.) (1996): *Mechanics of Poroelastic Media*, Kluwer Academic Publ., Dordrecht, The Netherlands.

Selvadurai, A.P.S. (2007a): The analytical method in geomechanics. *Applied Mechanics Reviews*, vol. 60, pp.87-106

Selvadurai, A.P.S. (2007b): Interface porosity and the Dirichlet/Neumann pore fluid pressure boundary conditions in poroelasticity. *Transport in Porous Media*, vol. 67. DOI 10.1007/s11242-007-9117-4 , pp 1-12.

Selvadurai, A.P.S.; Nguyen, T.S. (1995): Computational modelling of isothermal consolidation of fractured porous media, *Computers and Geotechnics* , 17, pp.39-73.

Selvadurai, A.P.S.; Shirazi, A. (2005): An elliptical disc anchor in a damage-susceptible poroelastic medium. *International Journal for Numerical Methods in Engineering*, vol. 63(14), pp. 2017-2039.

Seyrafian, S.; Gatmiri, B.; Noorzad, A. (2006): Green Functions for a Continuously Non-homogeneous Saturated Media. *CMES: Computer Modeling in Engineering & Sciences*, vol. 15(2), pp. 115-126.

Tan, S.-A.; Liang, K.-M.; Yong, K.-Y.; Lee, S.-L. (1992): Drainage efficiency of sand layer in layered clay-sand reclamation. *Journal of Geotechnical Engineering*, vol. 118(2), pp. 209.

Thimus, J.F.; Abousleiman, Y.; Cheng, A.H.-D.; Coussy, O.; Detournay, E. (Eds.) (1998): *Poromechanics, Proc. Biot Conference on Poromechanics*, A.A. Balkema, The Netherlands.

Ward, W.H.; Marsland, A.; Samuels, S.G. (1965): Properties of London clay at Ashford common shaft- In-situ and undrained strength tests. *Geotechnique*, vol. 15(4), pp. 321-344.

Wong, J.C. (1997): Model Studies of Lumpy Fill, *Master Thesis*, National University of Singapore.

Yang, L.-A.; Tan, T.-S.; Tan, S.-A.; Leung, C.-F. (2002): One-dimensional self-weight consolidation of a lumpy clay fill. *Geotechnique*, vol. 52(10), pp. 713-725.

Yang, L.-A.; Tan, T.-S. (2005): One-dimensional consolidation of lumpy clay with non-linear properties. *Geotechnique*, vol. 55(3), pp. 227-235.